IEEE Robotics and Automation Letters (RAL) paper presented at the
2020 IEEE/RSJ International Conference on Intelligent Robots and Systems (IROS)
October 25-29, 2020, Las Vegas, NV, USA (Virtual)

Fluid-structure Interaction Hydrodynamics Analysis on a Deformed Bionic Flipper with Non-uniformly Distributed Stiffness

Jinguo Huang[1,2,4], Yilun Sun[2], Tianmiao Wang[1], Tim C. Lueth[2], Jianhong Liang[1*] and Xingbang Yang[3*]

***Abstract*— Although the biologically flexible flippers of the cormorant (*Phalacrocorax*) are believed to be one of the most important features to achieve optimal swimming performance before take off, studies on a deformable bionic flipper with a non-uniformly distributed stiffness are rare. In this paper, to gain the unsteady hydrodynamic distribution between flexible aquatic animals and the ambient medium during the power stroke and recovery stroke, the numerical physical model solutions which coupled fluid-structure interaction based on computational fluid dynamics (FSI-CFD) are presented. We quantified the three-axis component distribution, and the results show that the horizontal force of the fluid will not provide positive thrust during the initial take-off stage. Greater lift and forerake moment are generated, which brings the body off the water as soon as possible and reduces the angle of attack. As the angle of attack decreases, the positive thrust will be generated, and the forward velocity and the lift will be further increased. As the draft area of the cormorant is reduced, the wings will start flapping, further increasing the lift and thrust, and thus taking off. The solver in the paper will serve as a framework for the future bio-inspired studies involving active and passive control associated with complex structural materials.**

I. Introduction

It has been widely recognized that swimming presents sophisticated and inspiring ventures in biomimetics and is expected to innovate new applications in biorobotics [1]–[4]. According to different bionic prototypes, the bionic underwater robot adopts different propulsion methods, such as imitating the jet propulsion of jellyfish achieved by shrinking their cavity [5], the fin propulsion of fish [6], [7], etc. Besides, the underwater propulsion methods of leg animals (such as lizards, frogs, etc.) are also discussed [8], [9]. A common feature associated with water birds swimming is that biological swimmers (e.g., cormorant) propel and control themselves in the water by oscillating their flippers and bodies [10], [11]. Real flippers possess the flexibility and therefore deform as they propel through the fluid. Swimming is usually accompanied by visible bending and torsion of the flexible flippers, which indicates the non-uniformly distributed stiffness performance (Fig. 1). On the other hand, the instantaneous shapes of the flippers have a profound influence on the fluid dynamic forces. It can be concluded that the interplay of the fluid dynamic and structure inertial forces may significantly improve the swimming performance (The water resistance is reduced about 2.5 times) [12], [13].

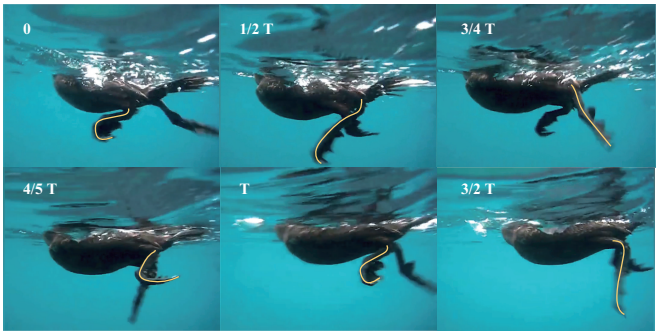

Fig. 1. Lateral view of observed flippers power and recovery strategies during cormorant swimming before take-off. Each image is cropped from one camera's full field of view. The cropped area does not change among panels, representing flipper motion relative to still water. The amphibious movements are achieved by the legs and flippers extending to propel the body forward. Meanwhile, the flippers travel in a lateral, backward arc relative to the body. Then the flippers begin to flex, bringing the legs forward and collapsing onto each other to accumulate forces for the next stroke [14]. The flipper recovery process is with the minimal angle of attack and area [15]. Noted that: the angle of attack was reduced for a take-off attitude adjustment while increasing the thrust

Therefore, to unveil novel mechanisms of natural swimming, we need to answer a central question on the physics of fluid-structure interaction (FSI) under various unsteady environments [16], in which the structure is subjected to the motion induced by the unsteady fluid forces. In return, the flow around the structure is also affected by the structural response [17]. Generally, elucidating the underlying mechanism of biological FSI locomotion involving the flexible deformation of aquatic animals relies on analyzing the physics of the interaction using numerical techniques [18] like Navier-Stokes equations (N-S equations), experimental study like observation visualization tools Particle Image Velocimetry (PIV) [19] and testing measurement [20]. Although the experimental approaches can deal with the biomimetic complexities in nature, in which the models can be constructed with different physical materials, they are still subjected to the availability of material diversity for conducting a systematic parametric study. Computational fluid dynamics (CFD) of swimming mechanical modeling allows us to directly solve the N-S equations, which govern biological fluid dynamics with the finite element methods (FEM). It can visualize swimming to provide detailed information on physical variables such as velocity and pressure at the macro- and microscopic level and hence give an overall understanding of the physical phenomena. The corresponding

*Corresponding authors: Jianhong Liang (robotics@buaa.edu.cn) and Xingbang Yang (xingbang@mit.edu).
[1]Robotics Institute, Beihang University, Beijing 100083, China
[2]Institute of Micro Technology and Medical Device Technology, Technical University of Munich, 85748 Garching, Germany
[3]MIT Media Lab, Massachusetts Institute of Technology, Cambridge, MA 02139-4307, USA
[4]Shen Yuan Honors College, Beihang University, Beijing 100083, China

structure mechanics equations can be solved by the elastic mechanics theory (EMT), to address the FSI gradually over time iteratively.

In the paper, we focus on the study of a flipper of the cormorant with complex variations of flexural rigidity, which coupled FSI based on CFD (FSI-CFD). Our research group has previously studied the two-phase flow hydrodynamics of the cormorant's flipper flapping on the water (power stroke) [21]. The bionic flipper was geometrically modeled as a deformable plate with curve fitting and parameter optimization, which is composed of the soft area connected to the rigid area. Combined with the FSI solver, more detailed flow field calculations have been carried out for the current research. At the same time, the large deformation calculations of the flipper in the recovery stroke are also obtained in FSI solver. The dynamic process of the initial stage before rapid take-off in the aspects of the flow characteristics and mechanical properties can be estimated in FSI-CFD.

II. Materials And Method

A. FSI-CFD solver Framework

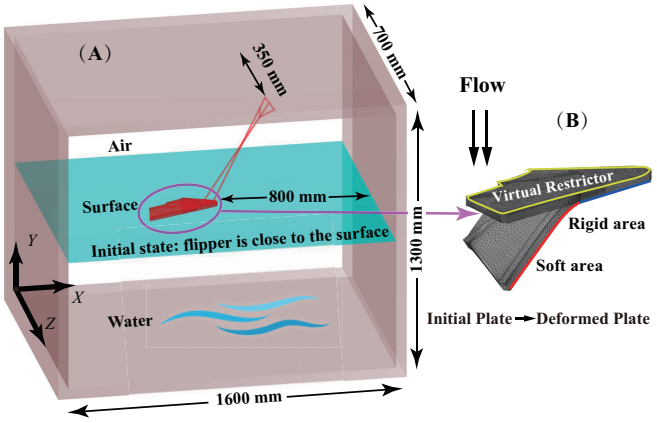

Fig. 2. A schematic representation of the flipper in the simulation computational domain. (A) Model setup for FSI of a flexible flipper immersed in water flow, including the sketch of geometric model dimension and coordinate setting. The calculation boundaries should be proper and not disturb the fluid movement around the flipper. Too vast boundaries will increase the grid amount and computational complexity; conversely, too cramped boundaries will limit the fluid motion and not correspond to reality. (B) Illustration of the flipper model where the soft area is attached to the rigid area, including the interaction between the surrounding fluid and flexible flipper, results in deformation. Note that the virtual restrictor in the software is set on one side of the flipper and restricts the flipper to deform only in one direction.

An integrated computational solver framework [21] based on FVM (Finite Volume Method) in *Ansys Fluent 19*, is applied in the paper to deal with the hydrodynamic problems of the deformable organism in two-phase flow. The above studies with live flipper experiments have some complexity and limitations due to the difficulties of controlling a real cormorant. To replicate the main morphological [22], kinematic [23] and dynamic [24] features of a real flipper in a computational simulation domain (Fig. 2(A)), an alternative way is to apply a bio-inspired robotic flipper with non-uniformly distributed stiffness [25], which has excellent mechanical properties [26]. In supplementary material, we demonstrate the preparation of mechanical backgrounds such as flipper morphology and kinematics.

The flipper which passes through both gas and liquid phases consists of a soft area as outlined in Fig. 2(B). The rectangular frame is the outside boundary in the calculated fluid domain (Fig. 3(A)), where the top boundary is pressure outlet which allowing free air circulation, and the others are slipping walls without viscosity. The vicinity grids of the flipper surface are compacted and performed with mesh nonuniform optimization (Fig. 3(B)). Meanwhile, the optimum grids were found from the grid independence test.

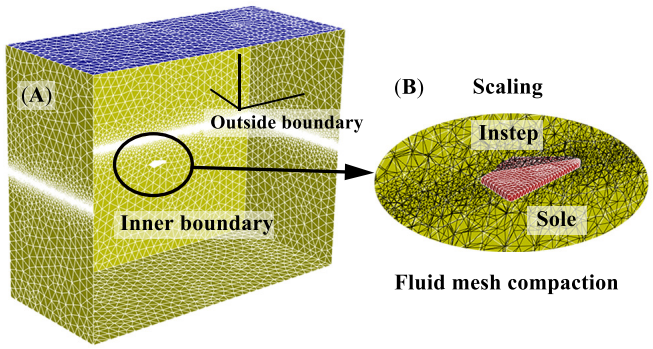

Fig. 3. Sketch of initially generated grids for global domain (A) and local compaction (B), including the numerical calculation parameters in both fluid mechanics and structure mechanics, respectively. The water-air interface is virtual and only used for illustration, whose position is calculated by the volume of fluid (VOF) gas-liquid two-phase method and grid mark tracking method [27]. Noted that the grids of the flipper surface in the fluid field are not consistent with those in the structure field. In FSI, force and displacement are transferred with interpolation between two fields.

The significance and settings of the virtual restrictor in the solver are as follows:

1. When the grids of soft area contact the virtual restrictor, the contact area will produce a rigid rebound effect on the soft area, thereby resisting the grids continuing to move in the direction of the restrictor and preventing them spatially overlapping. It is because the cormorant's flipper can only bend in one direction with non-uniformly distributed stiffness like the human's palm.
2. Neither the virtual restrictor nor the linkage needs to be gridded, so they do not directly participate in the FSI calculation. Therefore, their position information is only used for the structure mechanics, and will not be transmitted to the fluid mechanics. It can be considered that the fluid "penetrates" virtual restrictor and linkage during the calculation process.

B. FSI-CFD solver Approach

In the paper, due to the high-velocity movement of the flipper, the inertia has a significant influence on the analysis of structural mechanics. Therefore, the transient dynamics based on the FEM is used for calculation. In the model, the flexible elastic deformation, inertia, soft body gravity, virtual restrictor, the geometric motion of the linkage mechanism

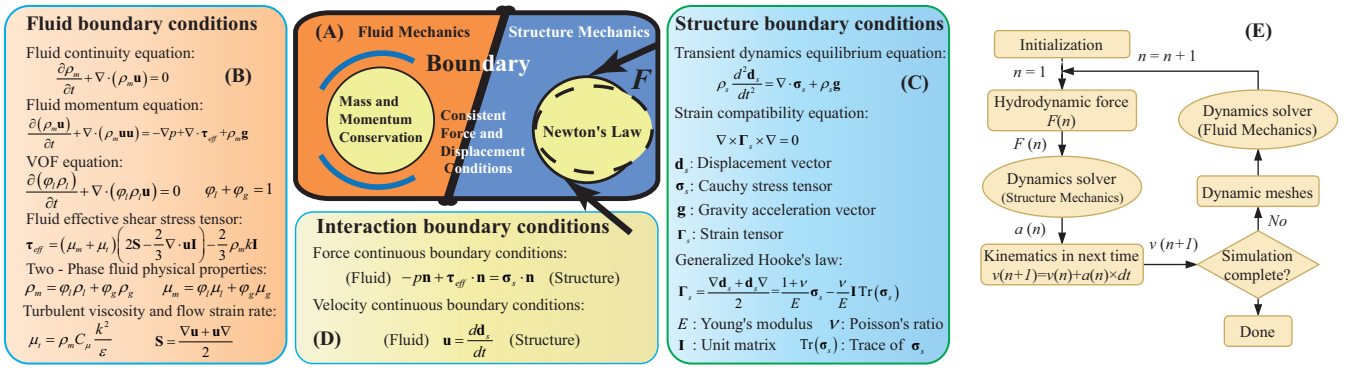

Fig. 4. FSI module boundary condition, data transfer correlation diagram and flow chart. The aerodynamic FSI solver needs to iteratively calculate the fluid and structure mechanics solution processes and advance the time to obtain the calculation results at each time point, which has been explained in the (A) diagram and (E) flowchart. The FSI mechanisms employed by flipper swimming before take-off are governed by (B) fluid boundary conditions, (C) Structure boundary conditions and (D) interaction boundary conditions.

and fluid force are considered. In fluid mechanics, the k-epsilon turbulence model, fluid gravity (buoyancy), and VOF gas-liquid two-phase flow model are used for calculation.

The biofluid dynamics of swimming, especially the bidirectional FSI process, is extremely complicated, and the interactions may play significant roles in the efficient natural locomotion. It is difficult to develop an accurate model to reveal all the effects of these factors. In the paper, the FSI-CFD numerical modeling is the partitioned approach, which is based on a staggered iteration [28]–[30]. Having performed the validation studies, we now demonstrate the versatility of the current numerical method for some practical applications. The main solution procedure of this method can be summarized as:

1. The hydrodynamic force is interpolated onto the structure surface, and then the structural elastic mechanics is solved;
2. The structure position and velocity are used to update the fluid field, and then the new hydrodynamic force can be obtained from the updated flow field.

1. and 2. are repeated until the results converge satisfactorily. Note that the iteration time step is 0.5 ms. The above content is explained in detail in Fig. 4. By inputting various constraint equations (Fig. 4 (B), (C) and (D)) in the computing simulation to set the calculation boundary conditions (Fig. 4(A)), the calculation process can be advanced automatically (Fig. 4(E)).

III. Result and Discussion

A. Velocity and Pressure distribution

We applied the developed FSI solver to the flexible flipper study aforementioned. A sequence of the flipper deformation patterns obtained from the present simulation is shown in supplementary video, where the different strokes are separated. The result shows that the flipper experiences spanwise and chordwise bending and also twisting deformations. These deformation characteristics are typical in insect wings [31] and fish fins [32], which are also consistent with the observations from our high-speed videos [23].

According to the dynamic characteristics of the flipper movement, this paper divides the motion into the following three strokes:

1. Aerial stroke (0 - 490 ms): The flipper moves in the air. The force and moment on the flipper are smaller due to the less density and viscosity, which can be ignored.
2. Power stroke (490 - 760 ms): The flipper moves backward in the water. The force and moment on the flipper are significantly greater than those in the aerial stroke due to the greater water resistance.
3. Recovery stroke (760 - 900 ms): The flipper moves forward in the water. The force and moment on the flipper are correspondingly greater than those in the power stroke due to higher speed.

When the flipper enters the water, air masses are brought into the water. The air masses shrink in the water as the flipper paddles. When the flipper moves to the lowest position in the water, it is completely immersed in the water. When it moves out of the water, because it cannot completely get out of the water, it will take out more water on the windward side. During the recovery stroke, the water even flows from the toe to the heel through the flipper surface.

The bionic flipper that moves on and within complex flowing environments can display both fluid and structure behavior in response to stress in the FSI-CFD. Since the flipper exhibits the characteristics of blunt body movement, the fluid resistance of the flipper is mainly geometrical resistance, and the frictional resistance can be ignored, which means that the pressure difference between the sole and instep surfaces can reflect the resistance of the flipper.

The pressure distribution has changed significantly from the power stroke. The main features are:

1. In the power stroke, the pressure on the sole firstly increases and then decreases, and the pressure at the center of the soft area (outer half) is the largest.
2. In the power stroke, the pressure on the instep firstly decreases and then increases, and the pressure at the edge of the rigid area (inner half) is the lowest, which is caused by the swirling vortex on the sole during the movement.

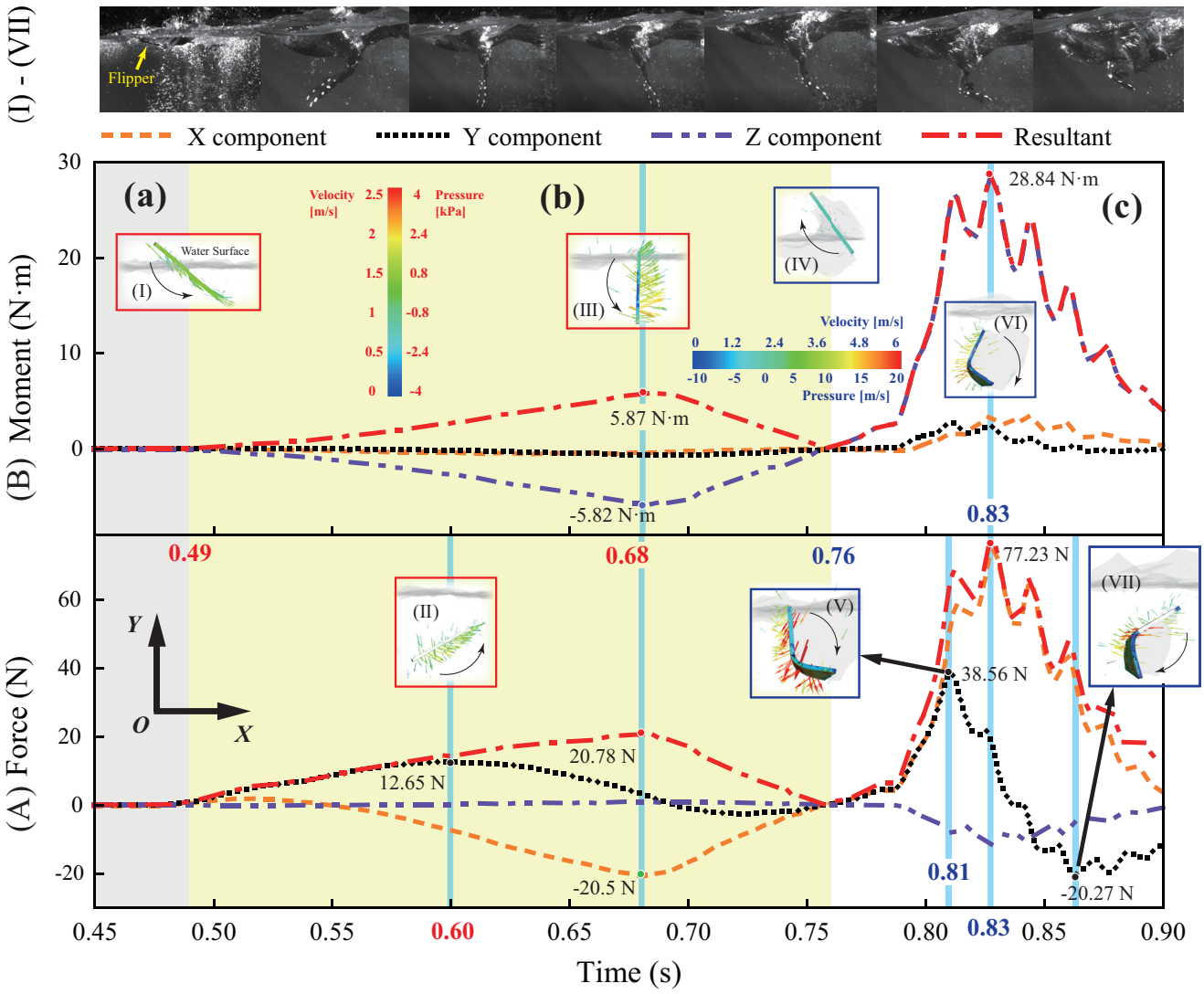

Fig. 5. Three-axis and the resultant descriptive changes about force (A) and moment (B) of the flipper in the (a) aerial stroke, (b) power stroke and (c) recovery stroke during the swimming process before cormorant take-off. At each stroke transition occasion and the time when obvious extreme points appear on the curve, we have given a schematic diagram of the velocity and pressure distribution. The red frames in (a) and (b) strokes correspond to the red counting reference legend. The blue frames in (c) stroke correspond to the blue counting reference legend. The Roman numerals I-VII represent the seven typical stages during the locomotion, showing the biological movement and fluid simulation movement in one-to-one correspondence.

3. In the recovery stroke, the pressure on the instep firstly increases and then decreases, and the soft area is significantly deformed under the water resistance. The area of maximum deformation is located at the edge of the soft area, which is exactly the point of upwind. The pressure in this area is also the largest in the spatial distribution of the sole. The deformation of the soft area reached its maximum at 820 ms, and the pressure reached its maximum at this moment, which was significantly greater than that in the power stroke.
4. In the recovery stroke, the pressure on the sole firstly decreases and then increases, and the pressure on the edge of the rigid area is the lowest.

B. Hydrodynamic analysis

Fig. 5(A) presents the three-axis and resultant force on the flipper.

1. In the aerial stroke, the force is negligible compared to other strokes.
2. After entering the water, force$_y$ reaches the maximum value in the power stroke at about 600 ms, and the maximum value in the recovery stroke at about 820 ms.
3. After entering the water, force$_x$ reaches the maximum value in the power stroke during about 640 - 680 ms and reaches the maximum value in the recovery stroke during about 830 - 850 ms.
4. The resultant force is basically the same as force$_x$.
5. Force$_z$ is in the order of 1 N in the power stroke, and in the order of 10 N in the recovery stroke, which can

TABLE I

COMPARISON OF IMPULSE, IMPULSIVE MOMENT, AVERAGE FORCE AND AVERAGE MOMENT ON THE FLIPPER

Period	Impulse$_x$(N·s)	Impulse$_y$(N·s)	Impulsive moment$_z$(N·m·s)	Average force$_x$(N)	Average force$_y$(N)	Average moment$_z$(N·s)
A	-0.004	-0.0006	-0.0009	-	-	-
P	-2.053	1.556	-0.714	-7.06	5.76	-2.64
R	4.035	0.159	1.709	14.94	0.59	6.33
W	0.026	1.079	0.113	0.096	3.996	0.420

* A: Aerial stroke (0 - 490 ms), P: Power stroke (490 - 760 ms), R: Recovery stroke (760 - 900 ms) and W: Whole time (0 - 900 ms). The value in the aerial stroke is too small, and all subsequent calculations are excluded.

be ignored compared with the resultant force and the impact of the asymmetry of the flipper is limited.

Fig. 5(B) presents the three-axis and resultant moment, whose reference point is the origin.

1. In the aerial stroke, the moment is negligible compared to other strokes.
2. The resultant moment is mainly dominated by moment$_z$, with limited influence from moment$_x$ and moment$_y$.
3. After entering the water, moment$_z$ reaches the maximum value in the power stroke during about 640 - 680 ms, which is to turn the cormorant hypsokinesis. Afterwards, the moment$_z$ reaches the maximum value in the recovery stroke during about 830 - 850 ms, which is to turn the cormorant forerake. The time at the maximum moment$_z$ is the same as that at the maximum resultant moment.

Note that X-axis points from the instep to the sole, thus the positive force$_x$ represents a hindrance to the forward movement of the cormorant. The impulse and impulsive moment in Table I reflect the cumulative time effects of fluid force and moment. According to the Momentum Theorem and Momentum Moment Theorem: Change of Impulse = Total Impulse, Change of Momentum Moment = Total Moment. Based on the integrated results in Table I, we can predict the changes in momentum and momentum moment of the cormorant's flipper as follows:

1. As with the conclusion of the force analysis, the fluid force and moment in the aerial stroke are relatively small and can be ignored.
2. Impulse$_y$ is positive after entering the water, which means that the fluid force can provide the flipper with a lifting effect to resist gravity. Impulse$_y$ in the power stroke is greater than that in the recovery stroke.
3. Impulsive moment$_z$ causes the cormorant hypsokinesis in the power stroke and forerake in the recovery stroke. Because the absolute value of the former is smaller than that of the latter, impulsive moment$_z$ dominates the turning of the cormorant forerake in the whole stroke.
4. After entering the water, impulse$_x$ will affect the horizontal movement of the cormorant. Impulse$_x$ is forward in the power stroke and backward in the recovery stroke. The absolute value of the latter is twice that of the former. Impulse$_x$ during the whole stroke is positive, meaning that the total effect of this series of actions is to reduce the momentum of the cormorant's forward movement, thereby the cormorant cannot obtain a net forward impetus through fluid force.
5. The recovery stroke is shorter than the power stroke, and the average force$_x$ in the recovery stroke can reach four times that in the power stroke.
6. The average force$_y$ is 3.996 N. So, both flippers can contribute nearly 8 N lift, and the weight of the cormorant is about 3 kg. As a rough estimate, the cormorant rises by about 10 cm if we assume that it has a balanced buoyancy and gravity during a treading period. It is close to the phenomenon we have observed, where the cormorant only needs the first cycle of flipper treading to make the wings emerge from the water and begin to flap in the next period.

At this stage, the flipper swims in the water to gain the impetus to take off. In the initial phase of take-off, the cormorant is more inclined to obtain a lift from the water. At the same time, the flipper captures a moment that makes the cormorant forerake, so that the angle of attack of the body gradually decreases, obtaining forward propulsion. As the draught area decreases, the wings of the cormorant begin to flap, further increasing the lift and thrust. Then the angle of attack started to increase gradually, and the lift coefficient subsequently increased, which further accelerates the take-off. The role of the flipper is producing the primary acceleration of take-off. The wings act when gaining a certain speed above the water surface, which is also evidenced by the conclusion of birds taking off on land [33].

IV. CONCLUSIONS

In this paper, we adopted a numerical solver to investigate the FSI-CFD in aquatic propulsion of flipper treading water during the cormorant takes off through a coupling of fluid mechanics with FEA and structure mechanics with EMT. The present solver can also be easily further applied by solving the hydrodynamics of molluscs, which pioneers the prospect of describing accurately mechanical characteristic of soft materials in FSI.

We then physically model the bionic prototype by addressing the morphology of the cormorant's flipper and obtain the input parameters of the dynamics simulation by analyzing the kinematics of the flipper. With a non-uniformly distributed stiffness along the surface of the flipper, real flipper deformation can be replicated. The unsteady hydrodynamic force and moment are correctly decomposed into three components,

and the obtained numerical modeling results are consistent with the previous experiment [34]. With the discussion of the relevant characteristics of biology, the impetus and attitude adjustment strategies of the cormorant in the take-off process are achieved, which are consistent with the observed phenomena (Fig. 1). The velocity and pressure flow field distribution are instructive to the improved design (including material selection and structural distribution), as well as the driving and control modes of bionic flippers.

As a final point, it is worthwhile to mention that further investigations on related topics are still necessary. The role of the passive response in the active swimming issues is worth further discussion, which highlights the extensions of FSI models to more complex and real configurations that remains challenging. In addition to bionic computing, we can achieve an equivalent surface deformation and an enhanced propulsion effect as a biologically active muscle-controlled flexible bionic flipper. Furthermore, it can not only analyze biological phenomena through bionic analysis, but also manufacture the bionic equipment that can genuinely realize the value of bionics.

ACKNOWLEDGMENT

This work was supported by the National Natural Science Foundation of China (51475028, 61703023), and the Graduate Innovation Practice Fund of Beihang University (YCSJ-01-201912). Many thanks to Dr. Sai Li for her encouragements and suggestions of the paper writing.

REFERENCES

[1] R. Pfeifer, M. Lungarella, and F. Iida, "Self-organization, embodiment, and biologically inspired robotics," *science*, vol. 318, no. 5853, pp. 1088–1093, 2007.

[2] X. Yang, T. Wang, J. Liang, G. Yao, and M. Liu, "Survey on the novel hybrid aquatic–aerial amphibious aircraft: Aquatic unmanned aerial vehicle (aquauav)," *Progress in Aerospace Sciences*, vol. 74, pp. 131–151, 2015.

[3] Y. Wang, X. Yang, Y. Chen, D. K. Wainwright, C. P. Kenaley, Z. Gong, Z. Liu, H. Liu, J. Guan, T. Wang, *et al.*, "A biorobotic adhesive disc for underwater hitchhiking inspired by the remora suckerfish," *Science Robotics*, vol. 2, no. 10, p. eaan8072, 2017.

[4] V. K. Venkiteswaran, L. F. P. Samaniego, J. Sikorski, and S. Misra, "Bio-inspired terrestrial motion of magnetic soft millirobots," *IEEE Robotics and automation letters*, vol. 4, no. 2, pp. 1753–1759, 2019.

[5] T. Hou, X. Yang, H. Su, B. Jiang, L. Chen, T. Wang, and J. Liang, "Design and experiments of a squid-like aquatic-aerial vehicle with soft morphing fins and arms," in *2019 International Conference on Robotics and Automation (ICRA)*. IEEE, 2019, pp. 4681–4687.

[6] J. Liang, T. Wang, and L. Wen, "Development of a two-joint robotic fish for real-world exploration," *Journal of Field Robotics*, vol. 28, no. 1, pp. 70–79, 2011.

[7] F. Xie, Z. Li, Y. Ding, Y. Zhong, and R. Du, "An experimental study on the fish body flapping patterns by using a biomimetic robot fish," *IEEE Robotics and Automation Letters*, vol. 5, no. 1, pp. 64–71, 2019.

[8] J. Glasheen and T. McMahon, "A hydrodynamic model of locomotion in the basilisk lizard," *Nature*, vol. 380, pp. 340–342, 1996.

[9] S. E. Peters, L. T. Kamel, and D. P. Bashor, "Hopping and swimming in the leopard frog, rana pipiens: I. step cycles and kinematics," *Journal of Morphology*, vol. 230, no. 1, pp. 1–16, 1996.

[10] K. Low, T. Hu, S. Mohammed, J. Tangorra, and M. Kovac, "Perspectives on biologically inspired hybrid and multi-modal locomotion," *Bioinspiration & biomimetics*, vol. 10, no. 2, p. 020301, 2015.

[11] A. Biewener and S. Patek, *Animal locomotion*. Oxford University Press, 2018.

[12] W. T. Gough, S. C. Farina, and F. E. Fish, "Aquatic burst locomotion by hydroplaning and paddling in common eiders (somateria mollissima)," *Journal of Experimental Biology*, vol. 218, no. 11, pp. 1632–1638, 2015.

[13] G. Ribak, D. Weihs, and Z. Arad, "Submerged swimming of the great cormorant phalacrocorax carbo sinensis is a variant of the burst-and-glide gait," *Journal of Experimental Biology*, vol. 208, no. 20, pp. 3835–3849, 2005.

[14] K. Schmidt-Nielsen, *Animal physiology: adaptation and environment*. Cambridge University Press, 1997.

[15] D. Schmid, D. Grémillet, and B. Culik, "Energetics of underwater swimming in the great cormorant (phalacrocorax carbo sinensis)," *Marine Biology*, vol. 123, no. 4, pp. 875–881, 1995.

[16] W.-X. Huang and S. Alben, "Fluid–structure interactions with applications to biology," *Acta Mechanica Sinica*, vol. 32, no. 6, pp. 977–979, 2016.

[17] H.-B. Deng, Y.-Q. Xu, D.-D. Chen, H. Dai, J. Wu, and F.-B. Tian, "On numerical modeling of animal swimming and flight," *Computational Mechanics*, vol. 52, no. 6, pp. 1221–1242, 2013.

[18] R. Li, Q. Xiao, Y. Liu, J. Hu, L. Li, G. Li, H. Liu, K. Hu, and L. Wen, "A multi-body dynamics based numerical modelling tool for solving aquatic biomimetic problems," *Bioinspiration & biomimetics*, vol. 13, no. 5, p. 056001, 2018.

[19] R. Alarcon, J. Allen, B. Thurow, A. Moss, *et al.*, "Development of a high-speed plenoptic imaging system and application to marine biology piv," *Measurement Science and Technology*, 2019.

[20] L. Wen, Z. Ren, V. Di Santo, K. Hu, T. Yuan, T. Wang, and G. V. Lauder, "Understanding fish linear acceleration using an undulatory biorobotic model with soft fluidic elastomer actuated morphing median fins," *Soft robotics*, vol. 5, no. 4, pp. 375–388, 2018.

[21] J. Huang, T. Wang, T. C. Lueth, J. Liang, and X. Yang, "Cfd based investigation on the hydroplaning mechanism of a cormorant's webbed foot propulsion," *IEEE Access*, vol. 8, pp. 31 551–31 561, 2020.

[22] X. Xue, X. Zhao, J. Huang, X. Yang, G. Yao, J. Liang, and D. Zhang, "Experiments and analysis of cormorants' density, wing loading and webbed feet loading," in *2016 IEEE International Conference on Robotics and Biomimetics (ROBIO)*. IEEE, 2016, pp. 83–87.

[23] J. Huang, X. Gong, Z. Wang, X. Xue, X. Yang, J. Liang, and D. Zhang, "The kinematics analysis of webbed feet during cormorants' swimming," in *2016 IEEE International Conference on Robotics and Biomimetics (ROBIO)*. IEEE, 2016, pp. 301–306.

[24] J. Huang, J. Li, H. Chen, X. Yang, J. Liang, and T. Wang, "Design and cfd based simulation analysis of a biotic webbed feet propulsion mechanism for hydroplaning," in *2018 IEEE International Conference on Robotics and Biomimetics (ROBIO)*. IEEE, 2018, pp. 83–87.

[25] C. Della Santina and D. Rus, "Control oriented modeling of soft robots: the polynomial curvature case," *IEEE Robotics and Automation Letters*, vol. 5, no. 2, pp. 290–298, 2019.

[26] S. Park, N. Jang, Y. S. Ihn, S. Yang, J. Jeong, S. Yim, S.-R. Oh, K. Kim, and D. Hwang, "A tele-operated microsurgical forceps-driver with a variable stiffness haptic feedback master device," *IEEE Robotics and Automation Letters*, 2020.

[27] C. W. Hirt and B. D. Nichols, "Volume of fluid (vof) method for the dynamics of free boundaries," *Journal of computational physics*, vol. 39, no. 1, pp. 201–225, 1981.

[28] F.-B. Tian, X.-Y. Lu, and H. Luo, "Propulsive performance of a body with a traveling-wave surface," *Physical Review E*, vol. 86, no. 1, p. 016304, 2012.

[29] R. Bhardwaj and R. Mittal, "Benchmarking a coupled immersed-boundary-finite-element solver for large-scale flow-induced deformation," *AIAA journal*, vol. 50, no. 7, pp. 1638–1642, 2012.

[30] G. Hou, J. Wang, and A. Layton, "Numerical methods for fluid-structure interaction—a review," *Communications in Computational Physics*, vol. 12, no. 2, pp. 337–377, 2012.

[31] R. J. Wootton, "Functional morphology of insect wings," *Annual review of entomology*, vol. 37, no. 1, pp. 113–140, 1992.

[32] M. Sfakiotakis, D. M. Lane, and J. B. C. Davies, "Review of fish swimming modes for aquatic locomotion," *IEEE Journal of oceanic engineering*, vol. 24, no. 2, pp. 237–252, 1999.

[33] K. D. Earls, "Kinematics and mechanics of ground take-off in the starling sturnis vulgaris and the quail coturnix coturnix," *Journal of Experimental Biology*, vol. 203, no. 4, pp. 725–739, 2000.

[34] J. Wang, O. M. Faltinsen, and C. Lugni, "Unsteady hydrodynamic forces of solid objects vertically entering the water surface," *Physics of Fluids*, vol. 31, no. 2, p. 027101, 2019.